

Confinement of PMo_{12} in Hollow $\text{SiO}_2\text{-}\text{PMo}_{12}\text{@rGO}$ Nanospheres for High Performance Lithium Storage

Hanbin Hu, Xueying Jia, Jiaxin Wang, Wei Chen,* Lei He* and Yu-Fei Song*

State Key Laboratory of Chemical Resource Engineering, Beijing Advanced Innovation Center for Soft Matter Science and Engineering, Beijing University of Chemical Technology, Beijing 100029, P. R. China. Email: songyf@mail.buct.edu.cn, helei@mail.buct.edu.cn, chenw@mail.buct.edu.cn; Tel/Fax: +86 10-64431832.

List of contents:

Fig. S1 SEM images (a) PMMA spheres and (b) PMMA@ SiO_2 spheres.

Fig. S2 FT-IR spectra of PMMA, PMMA@ SiO_2 , $\text{SiO}_2\text{-NH}_2$, PMo_{12} and $\text{SiO}_2\text{-}\text{PMo}_{12}$.

Fig. S3 (a) XRD patterns of $\text{SiO}_2\text{-}\text{PMo}_{12}\text{@rGO}$ and $\text{SiO}_2\text{@rGO}$. (b) TG curves of $\text{SiO}_2\text{-}\text{PMo}_{12}\text{@rGO}$, rGO and PMo_{12} .

Fig. S4 High-resolution XPS spectrum of P 2p peak of the $\text{SiO}_2\text{-}\text{PMo}_{12}\text{@rGO}$

Fig. S5 High-resolution XPS spectra of Mo 3d and P 2p peaks of PMo_{12} .

Fig. S6 The charge-discharge profiles for different cycles of $\text{SiO}_2\text{-}\text{PMo}_{12}\text{@rGO}$ under 100 mA g^{-1} .

Fig. S7 (a) The CV of the $\text{SiO}_2\text{@rGO}$; (b) The charge-discharge profiles for different cycles of $\text{SiO}_2\text{@rGO}$ under 100 mA g^{-1} ; (c) Rate performance of $\text{SiO}_2\text{@rGO}$ electrode; (d) Cycling performance and CE of $\text{SiO}_2\text{@rGO}$ under 100 mA g^{-1} within a voltage of 0.01-3.0 V.

Fig. S8 (a) The CV of the $\text{SiO}_2\text{-}\text{PMo}_{12}$. (b) The charge-discharge profiles for different cycles of $\text{SiO}_2\text{-}\text{PMo}_{12}$ under 100 mA g^{-1} . (c) Rate performance of $\text{SiO}_2\text{-}\text{PMo}_{12}$ electrode. (d) Cycling performance and CE of $\text{SiO}_2\text{-}\text{PMo}_{12}$ under 100 mA g^{-1} within a voltage of 0.01-3.0 V.

Fig. S9 TEM image of $\text{SiO}_2\text{-}\text{PMo}_{12}\text{@rGO}$ after 100 cycles at 100 mA g^{-1} .

Table S1. Comparison of $\text{SiO}_2\text{-}\text{PMo}_{12}\text{@rGO}$ with other reported SiO_2 - and POM-based electrodes as LIBs anode materials.

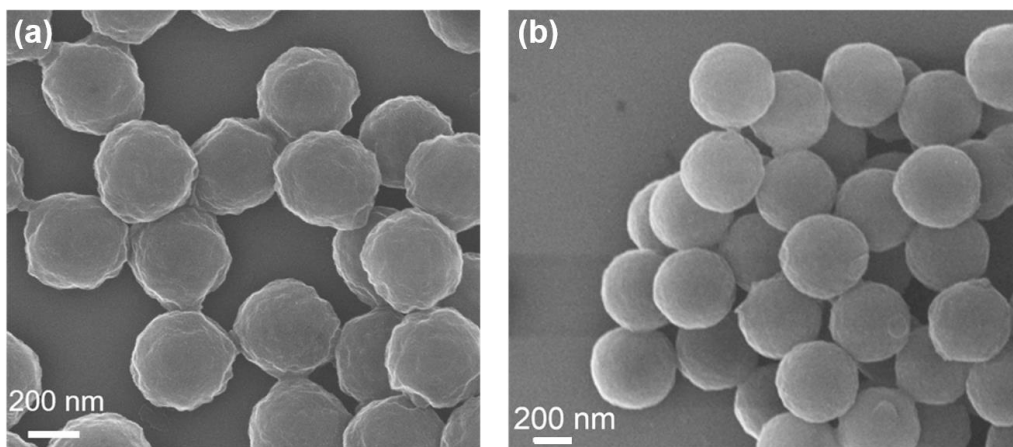


Fig. S1 SEM images of (a) PMMA spheres and (b) PMMA@SiO₂ spheres.

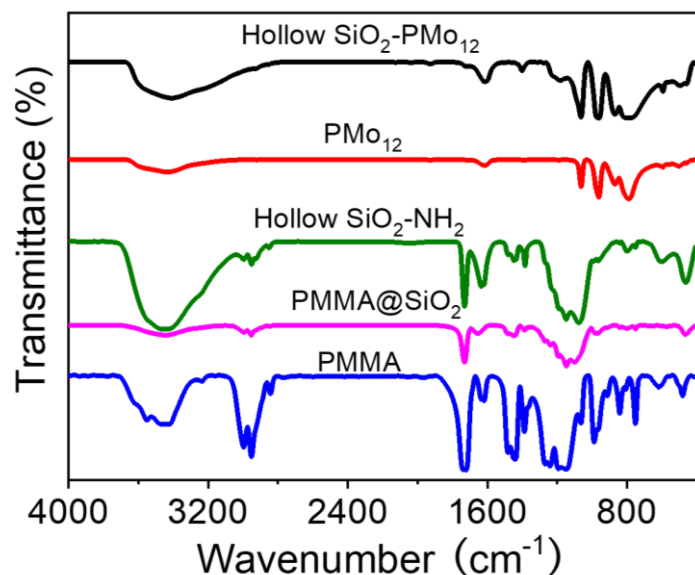


Fig. S2 FT-IR spectra of PMMA, PMMA@SiO₂, SiO₂-NH₂, PMo₁₂ and SiO₂-PMo₁₂, respectively.

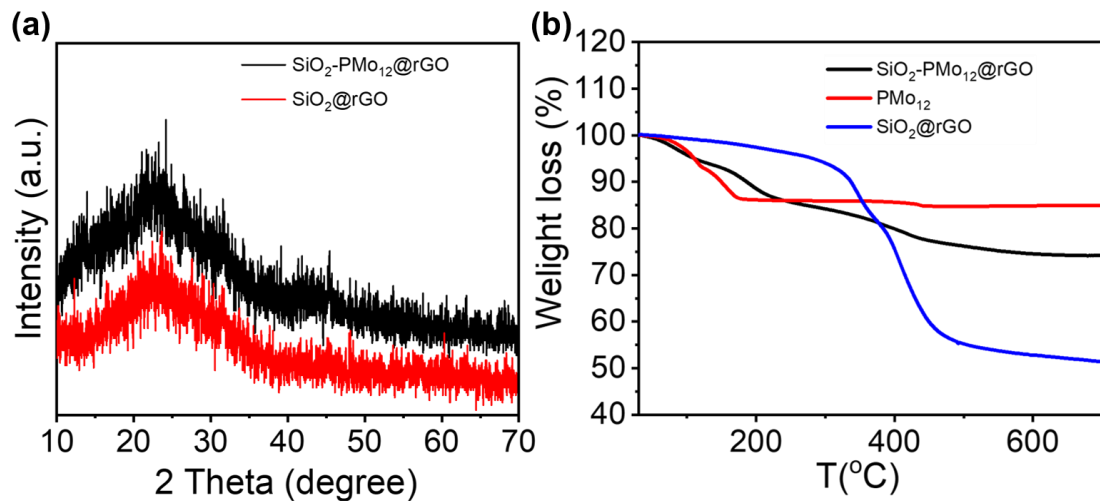


Fig. S3 (a) XRD patterns of $\text{SiO}_2\text{-PMo}_{12}\text{@rGO}$ and $\text{SiO}_2\text{@rGO}$. (b) TG curves of $\text{SiO}_2\text{-PMo}_{12}\text{@rGO}$, rGO and PMo_{12} .

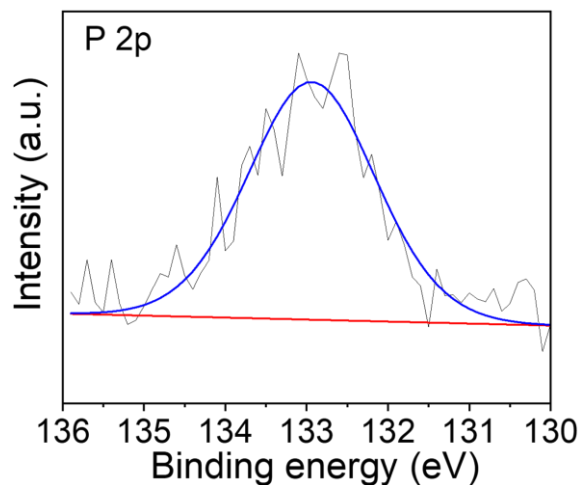


Fig. S4 High-resolution XPS spectrum of P 2p peak of the $\text{SiO}_2\text{-PMo}_{12}\text{@rGO}$.

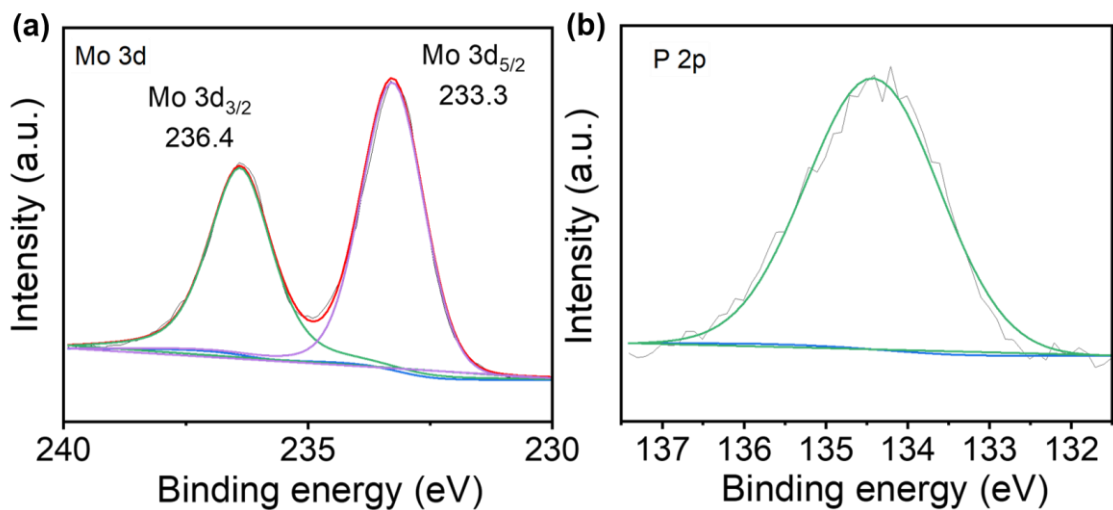


Fig. S5 High-resolution XPS spectra of Mo 3d and P 2p peaks of PMo₁₂.

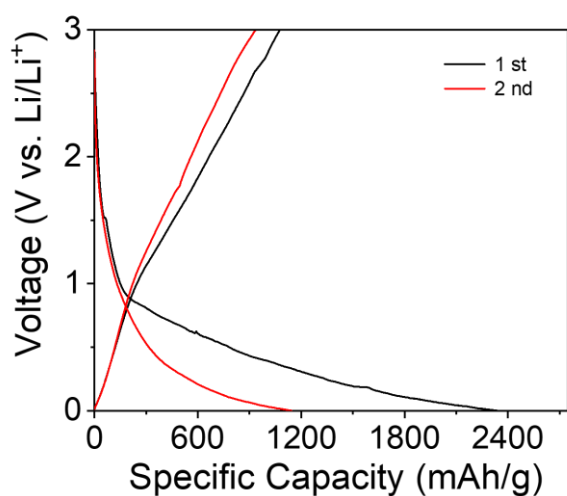


Fig. S6 The charge-discharge profiles for different cycles of SiO₂-PMo₁₂@rGO under 100 mA g⁻¹.

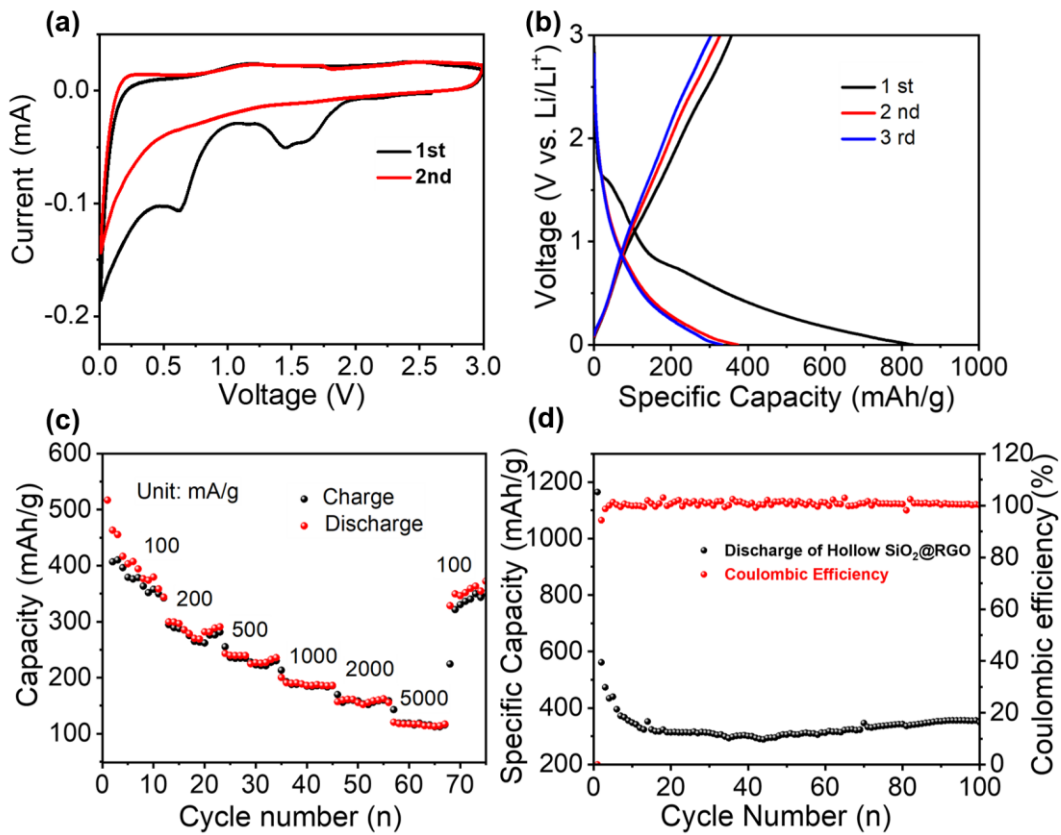


Fig. S7 (a) The CV of the SiO₂@rGO; (b) The charge-discharge profiles for different cycles of SiO₂@rGO under 100 mA g⁻¹; (c) Rate performance of SiO₂@rGO electrode; (d) Cycling performance and CE of SiO₂@rGO under 100 mA/g within a voltage of 0.01-3.0 V.

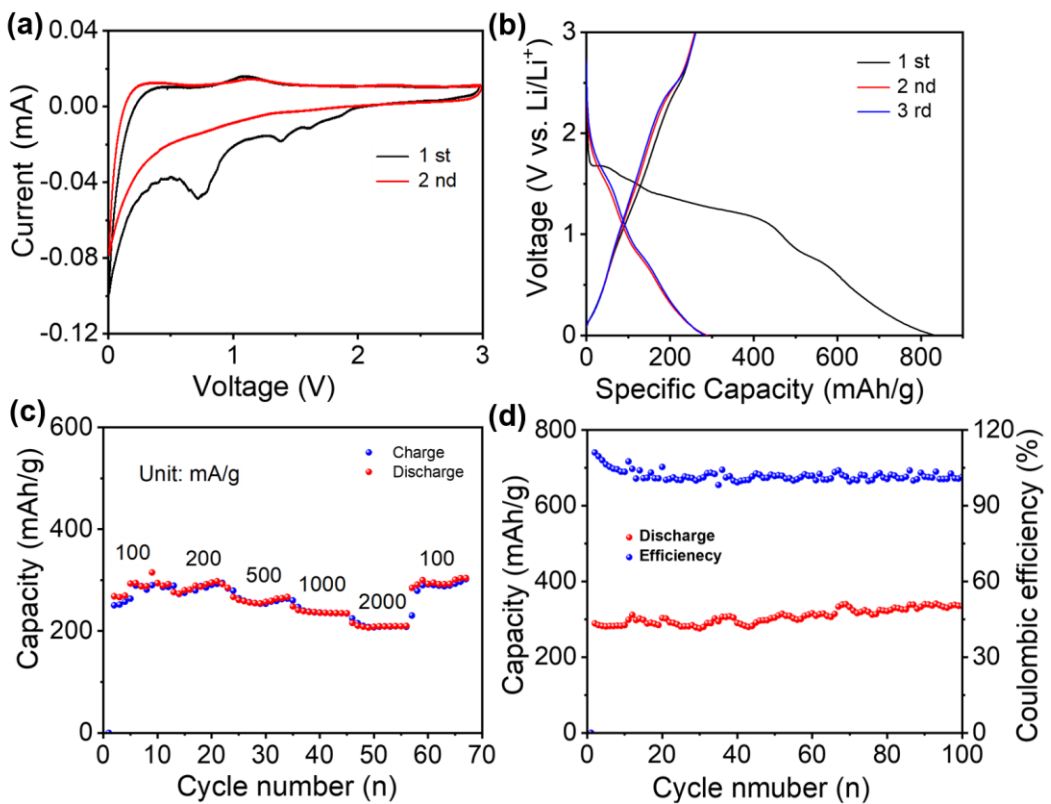


Fig. S8 (a) The CV of the $\text{SiO}_2\text{-PMo}_{12}$. (b) The charge-discharge profiles for different cycles of $\text{SiO}_2\text{-PMo}_{12}$ under 100 mA g^{-1} . (c) Rate performance of $\text{SiO}_2\text{-PMo}_{12}$ electrode. (d) Cycling performance and CE of $\text{SiO}_2\text{-PMo}_{12}$ under 100 mA g^{-1} within a voltage of $0.01\text{-}3.0 \text{ V}$.

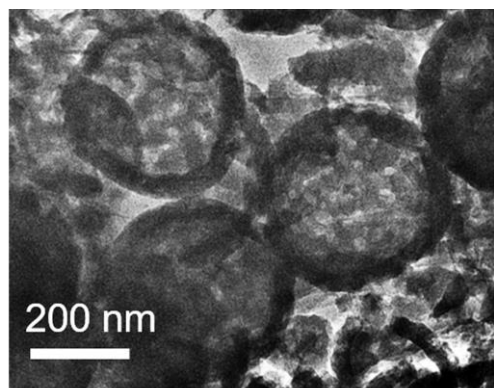


Fig. S9 TEM image of $\text{SiO}_2\text{-PMo}_{12}\text{@rGO}$ after 100 cycles at 100 mA g^{-1} .

Table S1. Comparison of $\text{SiO}_2\text{-PMo}_{12}\text{@rGO}$ with other reported SiO_2 - and POM-based electrodes as LIBs anode materials.

Electrode materials	Current density (mA g^{-1})	Capacity (mA h g^{-1})	Cycles	Ref.
Hollow $\text{SiO}_2\text{@CN}$	100	800	100	1
$\text{C/SiO}_2\text{/C}$	300	300	70	2
$\text{SiO}_2\text{/C}$ hollow spheres	100	624	100	3
H- $\text{SiO}_2\text{/C}$	200	564	400	4
CoW-POM-Cu foam	100	737	100	5
Py-Anderson-CNTs	0.5 mA cm^{-2}	665	100	6
$\text{PMo}_{12}\text{-PPy/RGO}$	100	1000	50	7
Hollow $\text{SiO}_2\text{-PMo}_{12}\text{@rGO}$	100	720	100	This work

References

1. T.T. Xiao, W.F. Zhang, T. Xu, J.X. Wu and M.D. Wei, Hollow SiO_2 microspheres coated with nitrogen doped carbon layer as an anode for high performance lithium-ion batteries, *Electrochim. Acta*, 2019, **306**, 106-112.
2. Z.Q. Gu, X.H. Xia, C. Liu, X. Hu, Y.X. Chen, Z.Y. Wang and H.B. Liu, Yolk structure of porous $\text{C/SiO}_2\text{/C}$ composites as anode for lithium-ion batteries with quickly activated SiO_2 , *J. Alloy. Compd.*, 2018, **757**, 265-272.
3. X.L. Liu, Y.X. Chen, H.B. Liu and Z.Q. Liu, $\text{SiO}_2\text{@C}$ hollow sphere anodes for lithium-ion batteries, *J. Mater. Sci. Technol.* 2017, **33**, 239-245.
4. Y. Jiang, D.B. Mu, S. Chen, B.R. Wu, Z.K. Zhao, Y.Z. Wu, Z.P. Ding and F. Wu, Hollow silica spheres with facile carbon modification as an anode material for lithium-ion batteries, *J. Alloy. Compd.* 2018, **744**, 7-14.
5. K. Sun, H.Q. Li, H.J. Ye, F.Q. Jiang, H. Zhu and J. Yin, 3D-Structured Polyoxometalate Microcrystals with Enhanced Rate Capability and Cycle Stability for Lithium-Ion Storage, *ACS Appl. Mater. Interfaces*, 2018, **10**, 18657-18664.
6. L. Huang, J. Hu, Y. Ji, C. Streb and Y.-F. Song, Pyrene-Anderson-modified CNTs as anode materials for lithium-ion batteries, *Chem. Eur. J.*, 2015, **21**, 18799-18804.
7. M. Zhang, T. Wei, A.M. Zhang, S.L. Li, F.C. Shen, L.Z. Dong, D.S. Li and Y.Q. Lan, Polyoxomolybdate-polypyrrole/reduced graphene oxide nanocomposite as high-capacity electrodes for lithium storage, *ACS Omega*, 2017, **2**, 5684-5690.